Euler Code Evaluation of a Transatmospheric Vehicle at Supersonic Speeds

Brian E. McGrath*
Lockheed Engineering and Sciences Company, Hampton, Virginia 23666
Peter F. Covell† and Steven X. S. Bauer
NASA Langley Research Center, Hampton, Virginia 23665
and
Ira J. Walker‡
Lockheed Engineering and Sciences Company, Hampton, Virginia 23666

An Euler code study has been conducted on a transatmospheric vehicle at Mach numbers from 1.5–4.5. The results show that the Euler code accurately predicted the lift, drag, and pitching-moment coefficients as a function of Mach number and angle of attack. The longitudinal stability characteristics were also predicted reasonably well as a function of Mach number. The code also predicted the changes in lift, drag, and pitching moment for forward and rearward shift of the wing from the nominal position. The Euler code provided an accurate prediction of the aerodynamic characteristics across the Mach-number range.

Nomenclature

$\bar{c}$ = mean aerodynamic chord, 14.4 in.
C_D = drag coefficient
$C_{D,0}$ = zero-lift drag coefficient
C_L = lift coefficient
C_{L_α} = $\partial C_L/\partial\alpha$, per degree
C_m = pitching-moment coefficient
C_{m_α} = $\partial C_m/\partial\alpha$, per degree
C_N = normal-force coefficient
C_{N_α} = $\partial C_N/\partial\alpha$, per degree
C_p = pressure coefficient
E,F,G = Euler equation fluxes
e = total energy per unit volume
L = reference length, 36 in.
M = freestream Mach number
p = pressure
Q = Euler equation dependent variable vector
S_{ref} = wing reference area, 116.6 in.^{2}
t = time
u,v,w = Cartesian velocity components
x_{cg} = moment reference center, $0.62L$
X_{cp}/L = zero-lift center of pressure location as a function of body length

$$\frac{X_{cp}}{L} = 0.62 - \frac{C_{m_\alpha}}{C_{N_\alpha}}\frac{\bar{c}}{L}$$

x,y,z = Cartesian coordinates
α = angle of attack
ρ = density
τ = transformed time coordinate

Presented as Paper 89-2193 at the AIAA 7th Applied Aerodynamics Conference, Seattle, WA, July 31–Aug. 2, 1989; revision received Feb. 2, 1991; accepted for publication Feb. 2, 1991.

*Senior Engineer, Aeronautics Department. Senior Member AIAA.
†Aerospace Engineer, Supersonic/Hypersonic Aerodynamics Branch, Applied Aerodynamics Division. Senior Member AIAA.
‡Principal Engineer, Aeronautics Department.

Introduction

VEHICLES that operate across the supersonic Mach-number range (Mach 1.5–5.0), such as missiles or transatmospheric vehicles, present a significant challenge to the aircraft designer. However, as a result of the development of advanced, higher-order aerodynamic prediction codes, better optimization of these types of vehicles can now be performed. The degree of optimization depends on the accuracy and range of applicability of the prediction methods employed. The recent development of generalized Euler analysis codes (Ref. 1, for example) represents a significant improvement over the linear theory or full-potential methods that have been previously used for supersonic vehicle design. The limitations of these linear theory and full-potential methods are described in Refs. 2 and 3.

In an effort to determine the capabilities of Euler aerodynamic prediction methodology, a computational study was performed in which Euler code predictions were compared with experimental results for a transatmospheric vehicle across the supersonic Mach-number range. The particular Euler equation solver used in this study is referred to as the Euler marching technique for accurate computation (EMTAC), developed by Szema, Chakravarthy, and Shankar at Rockwell International.[1] The configuration chosen for this study is representative of a recent transatmospheric vehicle design, which is readily amenable for geometric modeling in the computer code due to its simple geometric shape. The experimental results used in the comparisons were obtained from wind-tunnel investigations[3,4] conducted in the NASA Langley Unitary Plan Wind Tunnel (UPWT).

Euler predicted and experimentally determined longitudinal aerodynamic characteristics were compared for Mach numbers between 1.5 and 4.5. Angles of attack up to 25 deg were investigated. In addition to the wing-body configuration, a body-alone configuration was also analyzed across the Mach-number range. Of particular interest was a study of the wing-body interference effects. Also, the effect of wing longitudinal position was investigated at Mach 2.5 and 4.5.

Discussion

Wind-Tunnel and Model Geometric Description

The wind-tunnel tests of the wing-body configuration were previously conducted in the NASA Langley UPWT.[3,4] This wind tunnel is a continuous-flow facility with a Mach-number

range from 1.5–4.6 and a Reynolds-number range of 1.0×10^6 to 6.0×10^6 per foot. The wind tunnel has two test sections: test section 1 has a Mach-number range from 1.5–2.9 and test section 2 has a Mach-number range from 2.3–4.6. A complete description of the wind tunnel is contained in Ref. 5. Both test sections were used to obtain the experimental data for the following Mach numbers: 1.5, 2.0, 2.5, 3.0, 3.5, 4.0, and 4.5. The nominal test Reynolds number was 2.0×10^6 per foot. The angle of attack was varied between -4 and 28 deg. Transition grit was applied near the nose and wing leading edge to ensure turbulent boundary-layer conditions over the model. The data obtained include all six aerodynamic force and moment components that have been adjusted to correspond to a condition of freestream static pressure acting on the model base.

Figure 1 shows a sketch of the wing-body configuration. The fuselage consists of a circular 5-deg half-angle conical forebody, a cylindrical midbody, and a circular 9-deg truncated conical boattail. An engine package would be located around the midbody, but was excluded from the present study. The wing is a 4%-thick diamond airfoil delta wing of aspect ratio 1. The model was also fitted with a delta wing that was shifted fore or aft 5% of body length from the nominal wing position shown in Fig. 1.

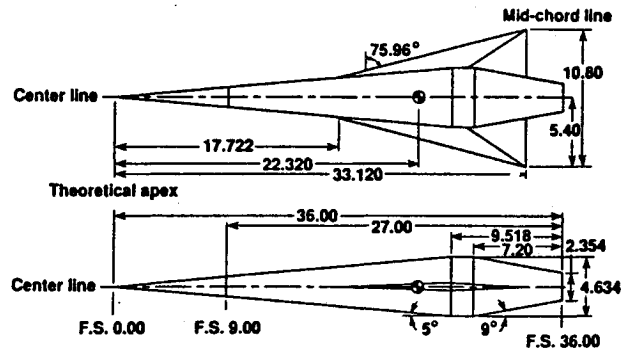

Fig. 1 Geometric description of the transatmospheric wing-body wind-tunnel model. All dimensions are in inches.

Code Description

EMTAC is the Euler version of a companion full-potential code called the supersonic implicit marching program (SIMP),[6] and is used exclusively for the theoretical analysis presented in this paper. The codes were written so that the similar user inputs, geometry, and gridding schemes are used for each code. Once familiar with one code, the user can easily adapt to application of the companion code. The user should become familiar with both codes[1,6] to best apply EMTAC.

The code uses a unified approach to solve the three-dimensional unsteady Euler equations. The governing equations are derived using a finite-volume discretization of the unsteady Euler equations. In conservation form, the Euler equations are

$$\boldsymbol{Q}_t + \boldsymbol{E}_x + \boldsymbol{F}_y + \boldsymbol{G}_z = 0 \tag{1}$$

where $\boldsymbol{Q}$, $\boldsymbol{E}$, $\boldsymbol{F}$, and $\boldsymbol{G}$ are defined as

$$\boldsymbol{Q} = \begin{bmatrix} e \\ \rho \\ \rho u \\ \rho v \\ \rho w \end{bmatrix}, \quad \boldsymbol{E} = \begin{bmatrix} (e+p)u \\ \rho u \\ \rho u^2 + p \\ \rho vu \\ \rho wu \end{bmatrix}$$

$$\boldsymbol{F} = \begin{bmatrix} (e+p)v \\ \rho v \\ \rho uv \\ \rho v^2 + p \\ \rho wv \end{bmatrix}, \quad \boldsymbol{G} = \begin{bmatrix} (e+p)w \\ \rho w \\ \rho uw \\ \rho vw \\ \rho w^2 + p \end{bmatrix} \tag{2}$$

and the total energy/volume is

$$e = \frac{p}{\gamma - 1} + \rho \frac{(u^2 + v^2 + w^2)}{2} \tag{3}$$

The code provides a steady-state solution of the Euler equations using a space-marching technique. An approximate factorization scheme is employed to obtain a steady-state solution for which an infinitely large time step $\Delta\tau$ is used in the supersonic portion of the flow. This makes the transient terms of the discretized unsteady equations vanish. In the subsonic part, a finite time step is employed; and the steady state is approached as a time asymptote using a planar relaxation method.

The flux vectors, $\boldsymbol{E}$, $\boldsymbol{F}$, and $\boldsymbol{G}$, are numerically represented by using a total variation diminishing (TVD) discretization based on Roe's scheme. The code formulation allows the user to obtain solutions for fully supersonic flow, supersonic flow with embedded subsonic regions, and subsonic flow. The shock regions are automatically captured by Roe's scheme and no special treatment is required.

Geometric Input

For geometrical input into the code, the body surface geometry must be defined for cross sections along the axial direction of the body. The surface geometry can be generated by various geometry packages or by an analytical definition of the surface geometry. The geometry is defined and input by dividing the cross section into various patches that best describe the surface. For the wing, body alone, and wing-body, the configuration is defined by four patches, two upper- and two lower-surface patches. The body can have a varying number of patches and can be defined accurately along a patch with a maximum of 30 definition points per patch. The grid package takes the surface input definition and uses a cubic spline to fit the surface points. The surface grid points along a patch are determined by the number of circumferential points selected by the user and are distributed evenly along a patch or clustered at either end of a patch. The gridding scheme then uses an elliptic grid solver to obtain the flowfield points between the surface and an outer boundary far enough away from the body to capture the bow shock.

Grid Resolution

A grid-resolution study was performed to give an indication of the sensitivity of the cross-sectional grid on the solution. The maximum cross-sectional grid currently available is 80 grid points along the surface circumference and 30 grid points normal to the surface (80×30) or 2400 cross-sectional grid points. For the grid-resolution study, the grid varied from near the maximum grid size (79×25) to a very coarse grid size (19×12). The axial step size was held constant at 0.1 in. and was based on the recommendations in Refs. 1 and 6. In addition, practical experience with EMTAC had shown very little sensitivity with small axial step size changes.

Cases were run on a Cray-2 at a Mach number of 3.0 for several angles of attack and grid densities. The grid chosen for presentation of the analysis was 61×20, which is 1220 cross-sectional grid points per marching step. The 61×20 grid was chosen because the grid provided good surface-geometry definition and reasonable surface pressure distributions. Also, the force coefficients were converged for grid densities greater than 1200 points per cross section. Furthermore, the grid

study indicated that the force coefficient and surface pressure distributions were more sensitive to grid variations in the circumferential direction than in the normal direction. Also, the study showed that 20 grid points normal to the body provided more than adequate resolution for the EMTAC calculations.

Results

The results presented in this paper consist of a discussion on the overall ability of the Euler code to predict the longitudinal aerodynamic characteristics of the wing-body configuration. For fully turbulent boundary-layer conditions, comparisons were made between predicted results and experimental wind-tunnel data. Additionally, a discussion will be included on the body-alone aerodynamic characteristics and the ability of EMTAC to predict interference effects for the wing-body combination. Lastly, a discussion on the effect of wing longitudinal position is included.

A skin-friction drag component was added to the inviscid Euler code results to facilitate comparison with the experimental data. The Sommer-Short method, which is described in Ref. 7, was employed to estimate the skin-friction drag assuming a fully turbulent boundary layer.

Figure 2 shows the longitudinal aerodynamic characteristics for the wing-body and body-alone configurations at $M = 2.5$. The Euler code shows good agreement with the experimental results for both configurations. The Euler code predicted the nonlinear lift increase that occurs for angles of attack between 10 and 15 deg. This nonlinear increase in lift is typical of cones.[8] Note, however, that a nonlinear decrease in lift is predicted at an angle of attack of about 20 deg, which was not observed experimentally. The drag polar comparisons show that the zero-lift drag and the drag due to lift are well predicted for both configurations. The pitching moments as a function of lift for both the wing-body and body-alone configurations show that the predictions are good for both configurations at most lift conditions ($C_L < 0.3$), with the exception of the wing-body at high-lift conditions. The nonlinear nose-up break in the pitch curve which occurs at $C_L \approx 0.2$ is slightly overpredicted for both configurations. These nonlinear trends in C_m are not typical of a conical body.[8]

Figure 3 shows longitudinal aerodynamic characteristics for the wing-body and body-alone configuration at $M = 4.5$. The computational results show good agreement for nearly the entire lift range with the exception of the highest lift conditions. The drag polars generally show good agreement at all

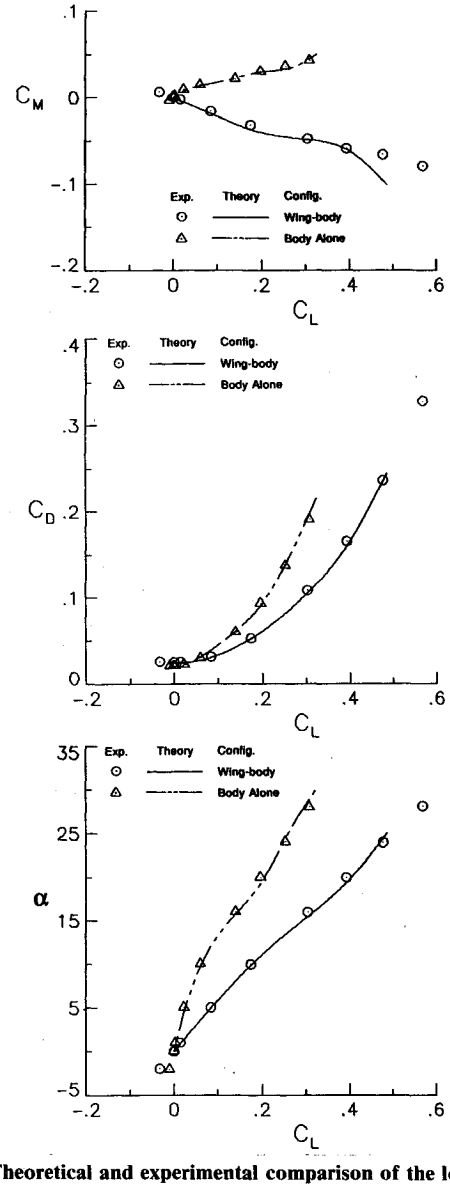

Fig. 2 Theoretical and experimental comparison of the longitudinal aerodynamic characteristics for the wing-body and body-alone configurations at $M = 2.5$.

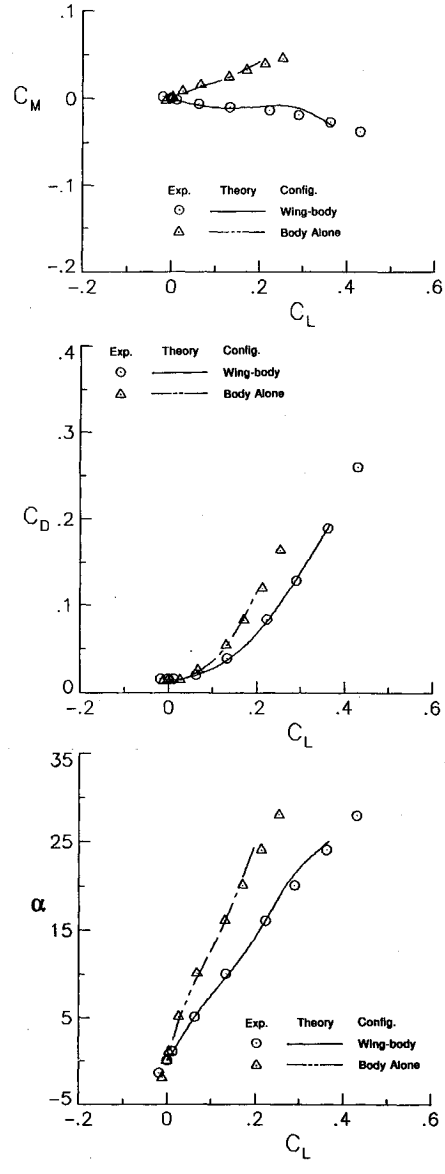

Fig. 3 Theoretical and experimental comparison of the longitudinal aerodynamic characteristics for the wing-body and body-alone configurations at $M = 4.5$.

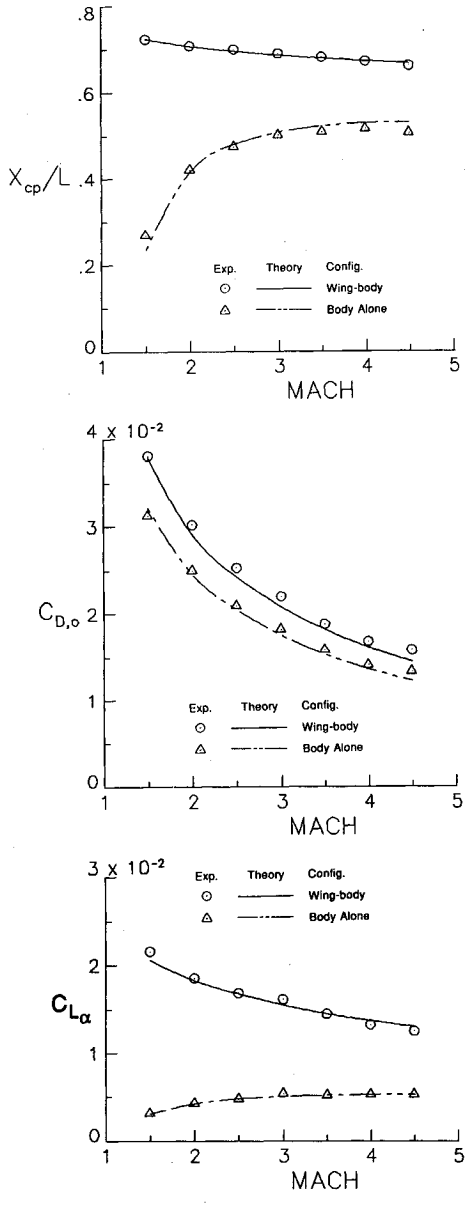

Fig. 4 Theoretical and experimental comparison of the Mach-number effects for the wing-body and body-alone configurations.

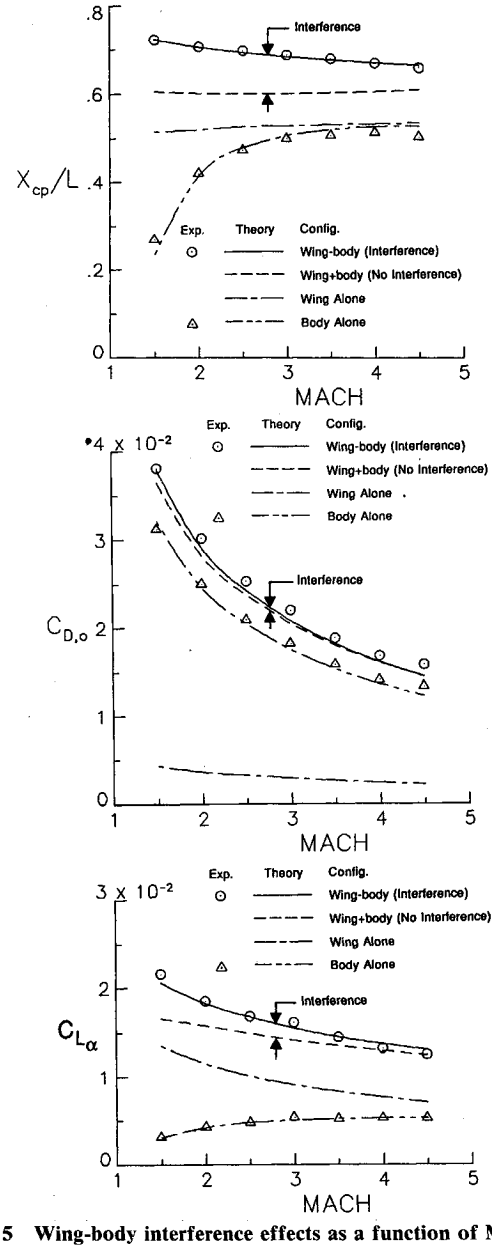

Fig. 5 Wing-body interference effects as a function of Mach number.

lift conditions. For the wing-body configuration the pitching moment is predicted reasonably well with the exception of the high-lift conditions ($C_L > 0.2$); and, for the body-alone configuration, the pitching-moment curve is reasonably predicted over all lift conditions.

Some of the discrepancies noted between the computational and experimental data may have to do with difficulties encountered while running the Euler code. The difficulties, numerical in nature, were encountered for the high-angle-of-attack cases while trying to ensure that the solutions were properly converged at each marching step. The signs of the problem were the existence of negative densities, a nonphysical flow property. Monitoring of the solution showed that the negative densities sometimes propagated throughout the flowfield causing the solution to diverge. Other cases showed that even with small regions of negative density the solutions still converged. Controlling the region or growth of the negative densities was done by varying several different input parameters to the code. These numerical problems were more difficult to control as both Mach number and angle of attack increased. Regions of negative density were usually located near the upper surface and along the leading edge of the geometry. Only the data at the highest lift conditions contained these small regions of negative density; however, even with these small regions of negative density within the flowfield, the solutions are presented here with confidence.

The Mach-number effects for the low angle-of-attack characteristics of the wing-body and body-alone configurations are shown in Fig. 4. For the wing-body configuration, the Euler code correctly predicted a 40% decrease in C_{L_α} between $M = 1.5$ and $M = 4.5$. For the body-alone configuration, the code also predicted a 7% increase in C_{L_α} from $M = 1.5$ to $M = 3.0$; and between $M = 3.0$ and $M = 4.5$, the code predicted the near-zero change in C_{L_α}. The zero-lift drag as a function of Mach number shows that the Euler code predicted the correct decrease in $C_{D,0}$ with increasing Mach number for both configurations, and also correctly predicted the increment in $C_{D,0}$ between the body-alone and the wing-body configurations. The absolute level of $C_{D,0}$ is slightly underpredicted at all Mach numbers for both configurations. A possible reason for this underprediction is that the viscous (Sommer-Short predicted, Ref. 7) component may be in slight error because the viscous calculation was performed using an equivalent exposed wing planform instead of the actual geometry. The location of the center of pressure as a percentage of body length (X_{cp}/L) shows that both the absolute levels

and Mach-number effects on X_{cp}/L are well predicted by the Euler code. It is important to note that the ability of the Euler code to accurately predict stability-related characteristics (in this case, X_{cp}/L) represents a significant improvement in capability over first-order prediction methods. Typically, the first-order methods do not accurately predict the stability characteristics.[3]

In Ref. 3, it was speculated that significant wing-body interference effects occurred. The Euler code was utilized to quantify these interferences effects (see Fig. 5). The wing-alone predictions are for the exposed wing planform. Adding the wing-alone to body-alone predictions yields the wing-body C_{L_α} with no interference. At $M = 1.5$, the favorable interference accounts for 21% of the total lift, but the favorable lift interference decreases as Mach number increases such that at $M = 4.5$ there is only a 3% interference increment. This is a typical Mach-number effect for wing-body interference.[9] The interference effect of $C_{D,0}$ is small as shown in Fig. 5. The interference on stability is reflected in the location of X_{cp}/L. The wing-body interference provides a large stabilizing effect across the Mach-number range. The stabilizing effect is seen by a 10% rearward shift in X_{cp}/L across the Mach-number range. The effect of interference on stability slightly decreases with increasing Mach number.

Comparison of the Euler code predictions with the experimental results for changes in wing longitudinal position at $M = 2.5$ is presented in Fig. 6. The Euler code predicted a decrease in lift at a given angle of attack for a rearward shift in wing position and an increase in lift at a given angle of attack for a forward shift in wing position. This effect of wing position on the longitudinal aerodynamic characteristics has been attributed to changes in the wing-body interference effects. The drag polars show the Euler code correctly predicted a collapse of the drag polars for all three wing positions at low lift ($C_L < 0.2$). The slight differences in drag due to lift are also correctly predicted. The pitching-moment comparison shows that the code correctly predicted the destabilizing effect for forward shift in wing position and the stabilizing effect for rearward shift in wing position. The nonlinear pitch-up trend that occurs at $C_L \approx 0.2$ is slightly overpredicted. Also, the Euler code overpredicted the pitching moment at the highest lift conditions for all three configurations.

Figure 7 shows the longitudinal aerodynamic characteristics as a function of wing position for $M = 4.5$. Again, the Euler

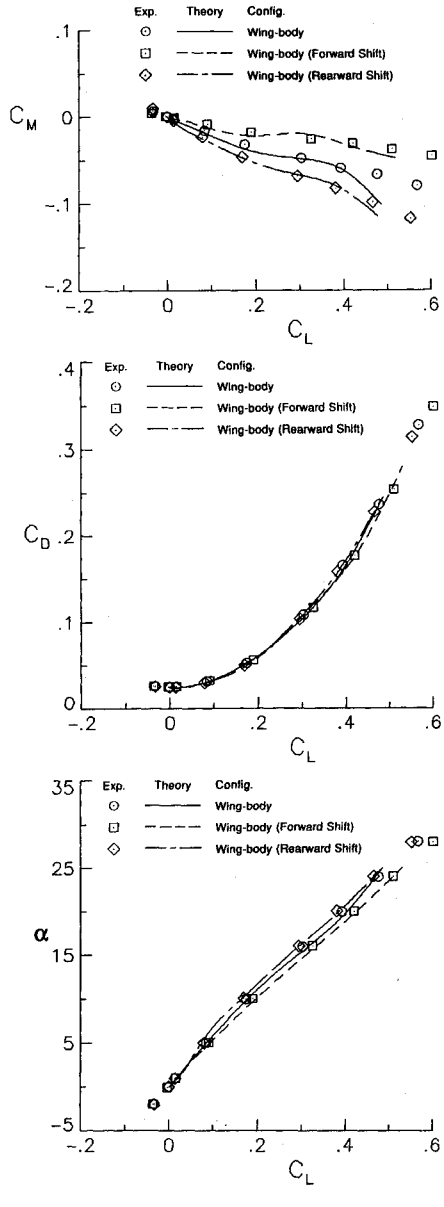

Fig. 6 Theoretical and experimental comparison of the longitudinal aerodynamic characteristics for variable wing position of the wing-body configuration at $M = 2.5$.

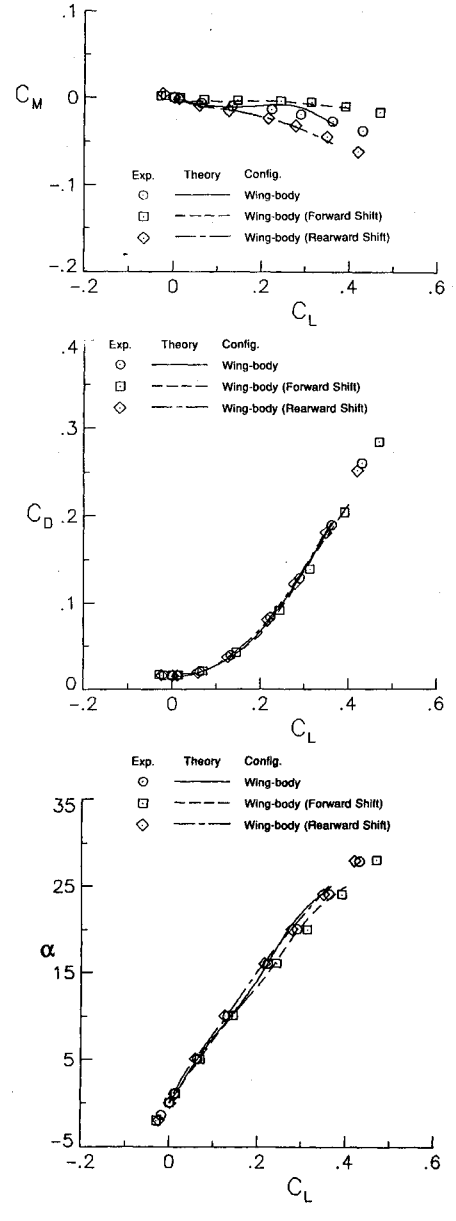

Fig. 7 Theoretical and experimental comparison of the longitudinal aerodynamic characteristics for variable wing position of the wing-body configuration at $M = 4.5$.

code predicted a decrease in lift for a rearward shift in wing position and an increase in lift for a forward shift in wing position at low lift. At the higher lift, the effect of wing position was not consistently predicted. The code correctly predicted the collapse of the drag polars for all three wing positions. The zero-lift drag levels also show excellent agreement. The collapse of the drag polars shows that the drag due to lift is the same as a function of wing position at $M = 4.5$. The pitching-moment coefficient shows that the code correctly predicted the decrease in nose-down pitching moment for a rearward shift in wing position. The code predicted a more nonlinear pitch curve for the nominal wing position.

Conclusion

A study was performed to evaluate the Euler code prediction capability on a transatmospheric vehicle in the supersonic speed regime. For fully turbulent boundary-layer conditions, comparisons were made between predicted results and experimental wind-tunnel data. Results show that the Euler code provided good prediction of the longitudinal aerodynamic characteristics for the wing-body and body-alone at $M = 2.5$ and $M = 4.5$. In particular, accurate prediction of the nonlinearities in lift and pitching moment were well-predicted. The effect of Mach number on C_{L_α}, $C_{D,0}$, and X_{cp}/L for the wing-body and body-alone configurations was accurately predicted over the Mach-number range of 1.5–4.5.

Predictions of wing-body interference showed that favorable increments in lift accounted for 21% of the lift at $M = 1.5$ and 3% of the lift at $M = 4.5$. Wing-body interference was responsible for a rearward shift in X_{cp}/L of about 10% body length at all Mach numbers.

Wing longitudinal position effects on lift curve slope, drag polar shape, and stability level were accurately predicted by the Euler code at $M = 2.5$ and $M = 4.5$. These results show that the Euler code can provide an accurate prediction of the longitudinal areodynamic characteristics for a slender transatmospheric vehicle over the entire supersonic speed range.

Acknowledgment

Thanks to Richard M. Wood of NASA Langley Research Center for his assistance and suggestions during the research for this paper.

References

[1]Szema, K., Chakravarthy, S., and Shankar, V., "Supersonic Flow Computations Over Aerospace Configurations Using an Euler Marching Solver," NASA CR-4085, July 1987.

[2]Pittman, J. L., and Siclari, M. J., "Nonlinear Aerodynamic Effects on Bodies in Supersonic Flow," AIAA Paper 84-0231, Jan. 1984.

[3]Covell, P. F., Wood, R. M., Bauer, S. X. S., and Walker, I. J., "Configuration Trade and Code-Validation Study on a Conical Hypersonic Vehicle," AIAA Paper 88-4505, Sept. 1988.

[4]Covell, P. F., Wood, R. M., Bauer, S. X. S., and Walker, I. J., "Experimental and Theoretical Evaluation of a Generic Wing Cone Hypersonic Configuration at Supersonic Speeds," Paper No. 83, 4th NASP Technology Symposium, Monterey, CA, Feb. 1988.

[5]Jackson, C. M., Corlett, W. A., and Monta, W. J., "Description and Calibration of the Langley Unitary Plan Wind Tunnel," NASA TP-1905, Nov. 1981.

[6]Shankar, V., Szema, K., and Bonner, E., "Full-Potential Methods of Analysis/Design of Complex Aerospace Configurations," NASA CR-3982, May 1986.

[7]Sommer, S. C., and Short, B. J., "Free-Flight Measurements of Turbulent-Boundary-Layer Skin Friction in the Presence of Severe Aerodynamic Heating at Mach Number from 2.8 to 7.0," NACA TN-3391, March 1955.

[8]Fournier, R. H., Spencer, B., Jr., and Corlett, W. A., "Supersonic Aerodynamic Characteristics of a Series of Related Bodies with Cross-Sectional Ellipticity," NASA TN D-3539, Aug. 1966.

[9]"Engineering Sciences Data Unit (ESDU): Method for Estimating the Normal-Force Coefficients of Delta Wing-Body Combinations at Supersonic Speeds at Incidences up to 25 Degrees," Data Item No. 68022, Dec. 1987.